Research Article | Vol. 14, No. 9 / 1 Sep 2023 / Biomedical Optics Express 4531
Biomedical Optics EXPRESS

Measuring intraocular pressure with OCT: the first approach

MARCELA NIEMCZYK* AND D. ROBERT ISKANDER

Department of Biomedical Engineering, Wroclaw University of Science and Technology, Wybrzeze Wyspianskiego 27, 50-370 Wroclaw, Poland
*marcela.niemczyk@pwr.edu.pl

Abstract: The variability of corneal OCT speckle statistics is indirectly related to changes in corneal microstructure, which may be induced by intraocular pressure (IOP). A new approach is considered, which attempts to estimate IOP based on corneal speckle statistics in OCT images. An area (A) under trajectories of contrast ratio with respect to stromal depth was calculated. The proposed method was evaluated on OCT images from the *ex-vivo* study on porcine eyeballs and *in-vivo* study on human corneas. A statistically significant multivariate linear regression model was obtained from the *ex-vivo* study: $\mathrm{IOP} = 0.70 \cdot A - 6.11$, in which IOP was precisely controlled in the anterior chamber. The *ex-vivo* study showed good correlation between A and IOP (R = 0.628, at the least) whereas the *in-vivo* study showed poor correlation between A and clinical air-puff tonometry based estimates of IOP (R = 0.351, at the most), indicating substantial differences between the two studies. The results of the *ex-vivo* study show the potential for OCT speckle statistics to be utilized for measuring IOP using static corneal imaging that does not require corneal deformation. Nevertheless, further work is needed to validate this approach in living human corneas.

1. Introduction

Measuring intraocular pressure (IOP) in the human eye has been a challenge that continues today [1,2]. Developed in the 1950s, Goldmann applanation tonometry is still considered the gold standard for measuring IOP, and serves as a benchmark for compatibility testing of other types of tonometers [3]. Non-contact tonometry currently focuses on devices that use concentrated air stream (air-puff), sufficiently strong to deform the cornea, and optical sensors to indirectly measure IOP. Their measurement uncertainty is high, their repeatability is low to moderate, and no standards have been developed for their calibration [4]. Such tonometers provide estimates of IOP that are termed *uncorrected* requiring the user to choose a range of correcting tables that include the confounding factors of central corneal thickness, age, and in some cases, the biomechanical parameters of the eye [5,6]. It should be noted that none of the tonometers used clinically measure IOP directly. To perform a direct measurement, a manometer is needed, which is connected to a syringe inserted into the anterior chamber of the eye. Such measurements have been performed intraoperatively [7], but are otherwise not feasible, because of safety and ethical reasons.

Optical coherence tomography (OCT) coupled with an air-puff system has been considered for determining corneal [8] and whole eye dynamics [9], evaluated at the instrument's axis, whereas multiple A-scan acquisitions are made in a short period of time (so called M-scan), during which the cornea is being deformed. Also, such a coupled system has been used for assessing corneal biomechanical properties [10]. Such systems are commonly termed as optical coherence elastography (OCE). The idea of measuring IOP with OCE has been contemplated recently [11].

Utilizing the statistical parameters of corneal OCT speckle in images statically acquired to indirectly assess the corneal microstructure has recently gained some attention [12,13]. An obvious extension of these studies was to consider the association of such OCT speckle parameters

#500546 https://doi.org/10.1364/BOE.500546
Journal © 2023 Received 14 Jul 2023; accepted 18 Jul 2023; published 9 Aug 2023

Biomedical Optics EXPRESS

with the level of IOP present in the anterior chamber and affecting the microstructure of the cornea [14]. However, the limitations of IOP being indirectly measured by non-contact tonometry was still a factor. A recent study involving freshly enucleated porcine eyes, which used a purposely constructed automated pressure system to control and maintain accurate IOP in the anterior chamber, showed a strong statistically significant relationship between IOP and speckle parameters estimated from OCT images of the central cornea [15]. That relationship was also strong when a non-parametric approach to OCT speckle analysis was used [16]. One such non-parametric statistic is the contrast ratio (CR), calculated in a given region of interest (ROI) as the ratio of the standard deviation of the speckle data to its mean [17].

Changes in IOP can be related to changes in corneal microstructure. The latter, consequently, can be indirectly imaged with OCT. Therefore, the aim of this study was to consider, for the first time, the idea of utilizing statistical information carried in corneal OCT speckle for measuring IOP.

2. Methods

2.1. Experimental data

Two retrospective data sets were analyzed. The first one included multiple OCT acquisitions of central porcine corneas from the recent *ex-vivo* study, in which an inflation test was performed on 23 whole porcine eyeballs, with IOP set and maintained at the levels from 10 to 40 mmHg, with a step of 5 mmHg. The IOP was precisely controlled and maintained at a given level directly in the anterior chamber using purposely designed setup equipped with a manometer. At each IOP level three non-averaged OCT B-scans were acquired sequentially without changing sample and instrument positions. Detailed description of the setup, as well as the experimental procedures, can be found in [15]. The porcine corneas involved in the study had central corneal thickness (CCT) between 800 μm and 950 μm.

The second data set consisted of OCT acquisitions of healthy human corneas from an *in-vivo* study. Subjects involved in this study were divided into two groups: OLD (age above or equal 50 years) and YOUNG (age range from 18 to 30 years). The exclusion criteria for the study were: history of ocular surgery within 12 months before the examination, intraocular diseases (e.g., diabetic retinopathy, macular degeneration), dry eye syndrome, or artificial ocular lens. Additionally, in cases of contact lens wear, subjects had to discontinue their use at least 24 hours before the examination. In the *in-vivo* study, the lowest CCT was 468 μm and 464 μm in the OLD and YOUNG group, respectively, and the greatest CCT was 628 μm and 633 μm, respectively. In the current study, subjects with CCT lower than 500 μm were also excluded. Additionally to OCT imaging, each subject had their IOP measured using a non-contact tonometer (Corvis ST, OCULUS, Wetzlar, Germany). The study was performed in accordance with the tenets of the Declaration of Helsinki and was approved by the institutional Ethics Board.

In both studies described above, the acquisition of corneal images was performed using spectral-domain OCT (SOCT Copernicus REVO 80, Optopol Technology, Zawiercie, Poland) with the central wavelength of 830 nm, half bandwidth of 50 nm, axial resolution of about 5 μm, and transversal resolution of 15 μm. Non-averaged OCT B-scans of the central cornea were collected, each of them composed from 12,036 A-scans. Scanning width was set to 5 mm, resulting in images with approximate resolution of 308 pixels/mm horizontally and 366 pixels/mm vertically.

2.2. Data processing

All analyses presented in this work were performed in MATLAB (MathWorks, Inc. Natick, MA, USA). In the preprocessing stage, the normalization of pixel values in OCT images was performed by dividing them by their maximum value of 255. Next, the inverse-log transformation

Biomedical Optics EXPRESS

was calculated as follows: $y = 10^x$, where x is the pixel value in the original image. Such transformed pixel values were again normalized according to the equation: $y' = (y - 1)/(10 - 1)$ where 1 (= 10^0) and 10 (= 10^1) correspond to the minimum and maximum possible pixel value after transformation, respectively.

2.2.1. *Ex-vivo* study on porcine corneas

To mark corneal layers, endothelium and top and bottom boundary of epithelium were delineated using the method described earlier in [12]. Next, the ROI encompassing part of corneal stroma was selected, with its top border placed 10 pixels below the lower boundary of the epithelium. As in the previous studies [15,16], the ROI width was set to 600 pixels (approximately 2 mm) to minimize the effect of geometrical distortion. An illustrative ROI with width W = 600 pixels and height H = 50 pixels is shown in Fig. 1. The position of ROI was being changed vertically within the stroma with a step of 5 pixels. The number of steps varied depending on corneal thickness, and in the last ROI position its bottom border was 10 pixels above the endothelium.

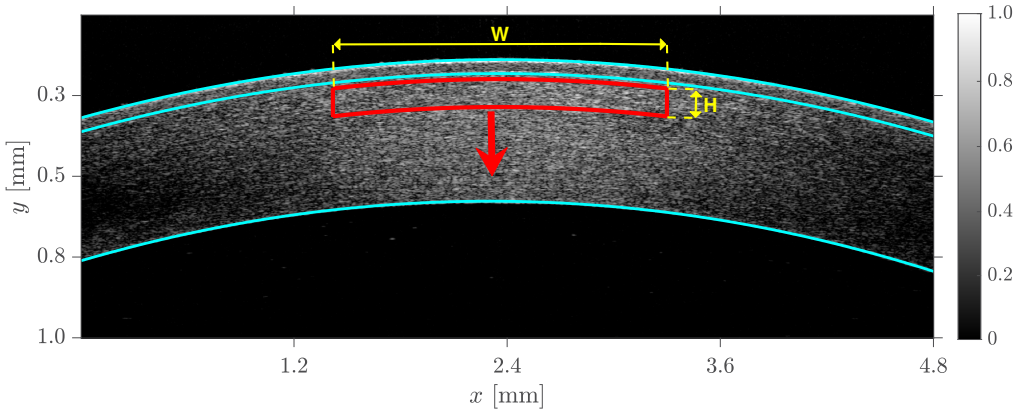

Fig. 1. Illustrative OCT scan of porcine cornea with endothelium and top and bottom boundary of epithelium, marked with cyan lines and moving ROI marked with red lines. Arrow indicates the direction of ROI movement. The yellow markings "W" and "H" indicate the width and height of ROI, respectively.

The analysis was performed on non-averaged OCT images. In the ex-vivo study three B-scans were acquired for each eyeball at each IOP level and estimates of CR were calculated for each ROI position. Further, median CR values for each set of three measurements were used to evaluate the CR trajectories as functions of stromal depth. The length of all trajectories was set to be equal to that of the shortest trajectory. The next step of the analysis was to search for parameters that would reflect the differences between CR trajectories for various IOP levels. Initially, the slope of each single trajectory was considered. This particular approach resulted in high statistically significant correlation between mean CR slopes and IOP (R = 0.997, p<0.001) [18]. However, when the correlation coefficient between these slopes and IOP values was calculated based on the model obtained using *multivariate* linear regression [19], the result was no longer statistically significant (R = 0.182, p = 0.406 for H = 20 pixels). It is important to stress that applying this type of regression allowed to take into account the relationship between consecutive measurements for each eyeball in the *ex-vivo* study.

In the second approach, all trajectories were first shifted down by subtracting the CR value calculated from the ROI in its first position. This operation allowed to reduce the impact of the variability of mean intensity of the images by analyzing only CR changes, not the values themselves. Then, the area under each such CR trajectory, denoted by A, was calculated using

Biomedical Optics EXPRESS

numerical integration via the trapezoidal method. The length of a trajectory was affecting the value of considered area, hence all trajectories were limited to be of equal length, corresponding to the shortest trajectory (i.e., that of the thinnest cornea). Correlation coefficient between the area under CR trajectory and IOP was calculated in the same manner as described earlier for the slope values, to estimate the parameters of a multivariate linear regression model.

2.2.2. *In-vivo* study on human corneas

In the *in-vivo* study, the calculation procedure for the area under CR trajectories was exactly the same as for the study on porcine eyeballs. For the Corvis ST measurements, a Dresden correction was applied to arrive at corrected IOP [20]

$$\mathrm{IOP}_{\mathrm{corr}} = \mathrm{IOP} + 23.28 - 0.0423 \cdot \mathrm{CCT}, \tag{1}$$

where IOP is the uncorrected IOP and CCT is the central corneal thickness, estimates which were provided by Corvis ST. Since no multiple measurements with varying IOP levels were available in this study, Pearson correlation coefficient was calculated between the area under CR trajectory and the corrected IOP, separately for the OLD and YOUNG group of subjects.

Eye positioning by the living human is never as precise as in the *ex-vivo* conditions due to the physiological eye and head movements. Thus, the position of the cornea in OCT images in this study varied between B-scans for different subjects. A short study on a phantom was performed to investigate how sample position affects speckle statistics. Also, partial correlation coefficient was calculated between IOP and area under CR trajectory with vertical cornea position set as a control variable.

2.3. Effect of sample position

To evaluate the effect of sample position on OCT speckle statistics, OCT images were acquired for different locations of a phantom made of epoxy resin mixed with blue dye particles. A set of such phantoms was used in the previous study [16] and here one of them was selected. The phantom was attached to a special holder and placed in front of the OCT instrument. After obtaining a good-quality OCT image of phantom in the preview of the device software, the position of the phantom was being changed by moving the holder using a micrometer screw and three non-averaged OCT images were acquired in each phantom position.

Figure 2 shows an illustrative OCT scan of the phantom used in this study. For every B-scan, the value of CR was calculated from the ROI of the size 600×180 pixels, placed 10 pixels below the top border of the phantom. Also, the CR trajectories were obtained by calculating CR value from ROI of size 600×20 pixels, moved vertically within the borders of the greater ROI with a step of 10 pixels. Area under CR trajectory was calculated in the same way as it was described in section 2.2.1. Sample position D was defined as a distance between top of the B-scan and top border of the phantom in OCT image.

Values of CR, as well as area under CR trajectory, are presented in Fig. 3. Strong correlation ($R = 0.917$, $p<0.001$) was obtained between CR and the sample position D, but the same was not observed for the area under CR trajectory ($R = 0.434$, $p = 0.211$). This indicates that CR values are sensitive to sample position in OCT imaging whereas the parameter, proposed in this study as a potential indicator of IOP, does not respond to changes in the position of the sample. The main reason for this lack of correlation is that the area under CR trajectory is normalized, as mentioned in section 2.2.1, with respect to the first ROI position, similarly to what was done in the works of Wang et al. [21] and Vilbert et al. [22] where speckle statistics of stroma were normalized by those of epithelium.

Biomedical Optics EXPRESS

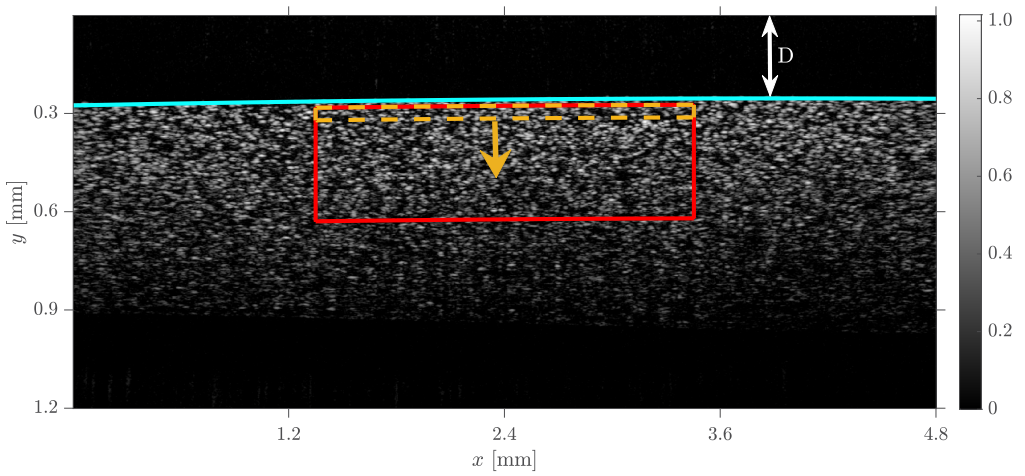

Fig. 2. Illustrative OCT scan of the phantom with two ROIs selected for the study. The single values of CR were calculated for pixel values from the greater ROI, marked with red lines, and the CR trajectories were obtained using a smaller, moving ROI, marked with orange dashed lines. The horizontal cyan line indicates the top surface of the phantom and the sample position, that is the distance between phantom surface and the top of the B-scan, is marked as D.

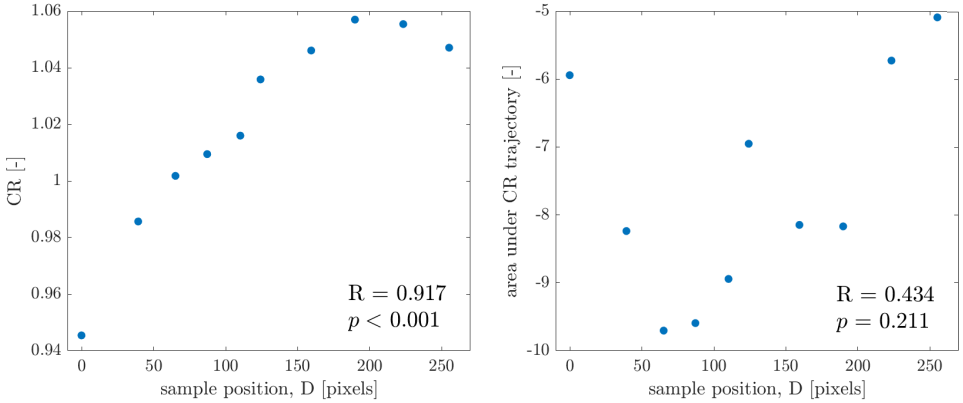

Fig. 3. Data for phantom. Values of CR (left) and the area under CR trajectories (right) for different positions of the phantom with respect to the OCT instrument. The correlation coefficients, together with their p-values, are presented in the bottom right corners of the plots.

3. Results

3.1. *Ex-vivo study on porcine corneas*

Based on the calculation of CR from pixel values within ROI in each position, the trajectories of CR changes were obtained for different IOP levels. These trajectories for group mean values of CR are presented in Fig. 4. The step of 20 pixels for moving ROI was used for better clarity of the plots. For the analysis presented in this work, the results obtained for the IOP of 10 mmHg were not taken into account since this IOP value is below the physiological level for porcine eyeballs (15 mmHg) [23,24], which may result in insufficient corneal tension, also affecting the statistical properties of speckle. The shape of presented trajectories is in general comparable

Biomedical Optics EXPRESS

between different ROI heights, although some differences can be observed in particular in CR values at the beginning of the trajectories.

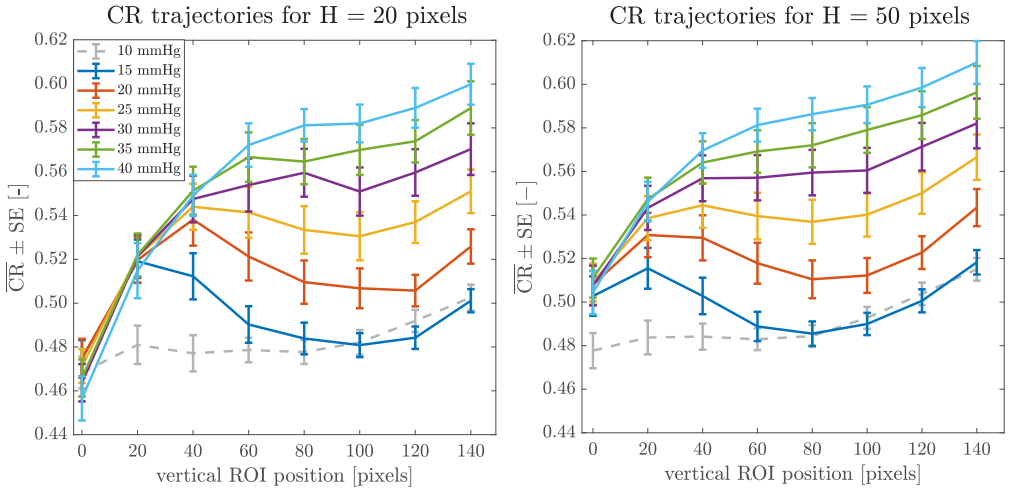

Fig. 4. Data for porcine eyeballs. Illustrative examples of mean trajectories of CR changes together with error bars representing standard error for IOP levels from 10 to 40 mmHg. The trajectories are presented for two illustrative ROI heights of 20 and 50 pixels. The trajectories at 10 mmHg (a non-physiological level of IOP) were excluded from further analysis.

The values of the correlation coefficient between the area under CR trajectories and IOP for different heights of ROI in the *ex-vivo* study on porcine eyeballs are shown in Table 1. The highest value of the correlation coefficient, equal to 0.720 (p<0.001), was obtained when ROI with H = 20 pixels was utilized. For this ROI size, Fig. 5 presents the boxplots together with group mean values of the area under CR trajectories. It shows that the area is increasing with IOP almost linearly and the Pearson correlation coefficient calculated between IOP and the group mean values of the area under CR trajectories was equal to 0.997 (p<0.001).

Table 1. Results of multivariate linear regression for the *ex-vivo* study on porcine eyeballs. Values of correlation coefficient R between IOP and area under CR trajectory and corresponding *p*-values for different ROI height H.

H [pixels]	R	p
5	0.689	<0.001
10	0.704	<0.001
20	0.720	<0.001
30	0.693	<0.001
40	0.646	<0.001
50	0.628	0.001

In search of a method of measuring IOP with OCT, one can, as a first approach, use the result of multivariate linear regression model to estimate IOP as

$$\text{IOP} = 0.70 \cdot A - 6.11, \tag{2}$$

where A is the estimator of the area under the CR trajectory, as described earlier. This initial result is valid for the study with porcine eyes and the particular acquisition protocol used in it, whereas for the human eyes such an approach needs to be verified in further studies.

Biomedical Optics EXPRESS

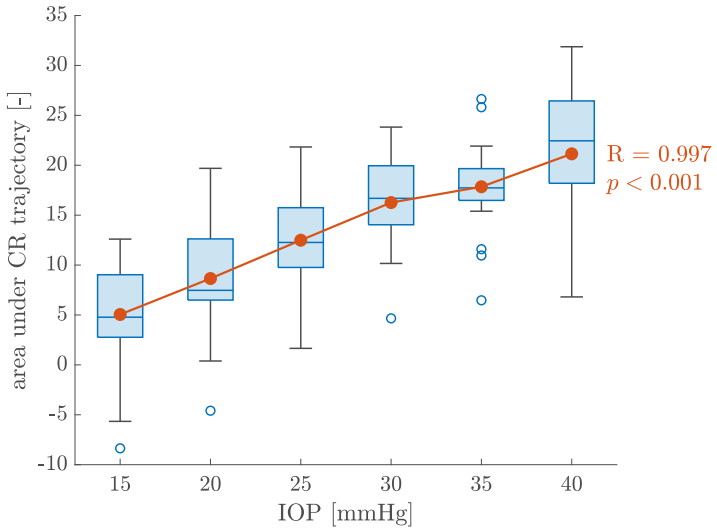

Fig. 5. Boxplots of the area under CR trajectories for IOP levels from 15 to 40 mmHg. Blue circles indicate outliers found using Tukey's method. Red markers connected by a line show group mean values of the area under CR trajectories and Pearson correlation coefficient between this area and IOP is presented together with its p-value.

3.2. *In-vivo study on human corneas*

In the *in-vivo* study on human corneas, 31 and 27 subjects were involved in the OLD and YOUNG group, respectively, with corresponding age ranges from 50 to 87 years and from 21 to 30 years.

Values of Pearson correlation coefficient between the area under CR trajectory and the corrected IOP values for different heights of ROI are presented in Table 2. No statistically significant correlations were found for all ROI heights in both, OLD and YOUNG, groups. In addition, it is worth noting that the trend is positive in the OLD group, while in the YOUNG group it is negative, which indicates that it is not possible to consider these two age groups jointly. This suggests that other confounding factors related to age may play role in those differences. To assess if the position of the cornea in OCT images is influencing speckle statistics and hence those correlations, partial correlation coefficient, with sample position set as a control variable, was also calculated and presented in Table 2. The results show that there are no considerable

Table 2. The results of correlation analysis for the *in-vivo* study on human corneas. Values of Pearson correlation coefficient R and partial correlation coefficient ρ between IOP and area under CR trajectory and corresponding *p*-values for different ROI height H, separately for OLD and YOUNG groups. For partial correlation the sample position was set as a control variable.

H [pixels]	OLD				YOUNG			
	R	p	ρ	p	R	p	ρ	p
5	0.318	0.081	0.332	0.073	−0.227	0.219	−0.098	0.635
10	0.351	0.053	0.340	0.066	−0.221	0.232	−0.098	0.633
20	0.318	0.081	0.266	0.156	−0.254	0.168	−0.169	0.409
30	0.167	0.369	0.094	0.620	−0.211	0.254	−0.151	0.463
40	0.178	0.338	0.090	0.638	−0.102	0.585	0.071	0.730
50	0.115	0.538	−0.012	0.950	−0.081	0.665	−0.143	0.488

Biomedical Optics EXPRESS

differences between Pearson and partial correlation coefficient values, so sample position is not supposed to affect considered speckle statistics significantly.

4. Discussion

In this study, a novel method of corneal OCT speckle analysis is presented. It is based on the evaluation of changes of statistical speckle parameters through the corneal stroma rather than the analysis of single values of such parameters, calculated from a specified ROI, as it was presented in previous works [15,16]. In this way the trajectories of parameter estimates with respect to stromal depth could have been considered. Those, in turns, facilitated an estimate of IOP derived entirely from static acquisitions of central cornea and a multivariate linear regression model.

Using CR for the indirect assessment of changes occurring in the structure of the imaged sample was considered in literature and CR values were shown to be linked to the density of scattering particles in the sample [17,25]. Li et al. [26] developed such an approach and showed changes in CR values with depth in a homogeneous sample. He also presented a theoretical model, verified experimentally, which revealed that for the superficial layer of the sample (approximately 700 μm), CR is a linear function of sample depth. Moreover, slope of this function is proportional to the scattering coefficient of the sample [27]. The cornea is an inhomogeneous tissue and it consists of collagen bundles organized in lamellae [28]. The arrangement of lamellae varies through the cornea [29], so it is supposed that the microstructure can influence CR values as well, as it was shown in the recent study of Danielewska et al. [30], where spectroscopy of cornea tissue samples was performed additionally to cornea OCT imaging. Further, it was shown that increasing IOP causes the reorganization of lamellae in the stroma [31]. Thus, the changes in CR trajectories for different IOP levels, observed in Fig. 4, are likely to be caused by the underlying rearrangement of collagen structure. Although the CR trajectories appear to vary for different ROI heights (see Fig. 4), the resulting correlations between IOP and the area under trajectory are not substantially different for the *ex-vivo* study. This indicates that optimization of the ROI height that maximizes such a correlation may not be demanding. Entirely different situation is observed in the *in-vivo* study, where the considered correlations were smaller than those in the *ex-vivo* study and statistically insignificant, pointing to substantial differences between the two sets of data (i.e., porcine and human eyes set), and the conditions at which they were acquired. Table 3 summarizes those differences. It is likely that by increasing the accuracy and precision of IOP measurement as well as having the opportunity to perform it directly in the anterior chamber, the results of correlation between speckle statistics and IOP would be higher than those currently achieved in the *in-vivo* conditions.

Table 3. Major differences between the two considered set of data and their measurement conditions.

Item	*ex-vivo*	*in-vivo*
Object	porcine eyes	human eyes
IOP technique	manometry	air-puff tonometry
IOP access	direct	indirect
IOP precision	high	low
IOP accuracy	high	low
IOP range	10 to 40 mmHg	12 to 22 mmHg

Hence, the study has some limitations. Firstly, the study concerns porcine eyes and the generalization of the results to human corneas cannot be undertaken without further investigations. Also, the range of IOP values in the *in-vivo* study is limited to normative IOP levels, whereas the *ex-vivo* study included potentially pathological levels of IOP, if applied to human eyes. Further,

Biomedical Optics EXPRESS

in the *ex-vivo* study, the values of IOP were precisely and accurately measured in the anterior chamber, whereas in the *in-vivo* study, estimates of indirectly measured IOP were used. This IOP measurement distinction resulted in high, for porcine eyes, and low, for human eyes, correlations of considered areas under the CR trajectories with IOP. Future studies with human subjects should include higher levels of IOP, preferably acquired during examination of pathological eyes [32], rather than obtained in studies where IOP is elevated artificially (e.g., during a water drinking test [33]).

Another significant difference between two considered studies is that in the *ex-vivo* study IOP was maintained at all times at the same level, whereas in the human eyes, the phenomenon of ocular pulse occurs, which modulates the values of IOP in accordance to signals of cardiopulmonary system. The variations in ocular pulse, generally termed ocular pulse amplitude (OPA), can reach several mmHg [34,35] and are known to vary during the day [36]. When considering ocular pulse in OCT imaging not only changes in IOP need to be taken into account, but also the corneal axial displacement, which typically has a peak-to-peak amplitude of about 40 μm [37,38] but may also reach almost 100 μm [39], when no bite-bar is administered during the measurements. For the OCT device used in this study this value results in a change of vertical cornea position in OCT image of approximately 37 pixels. The study on phantom, described in section 2.3, revealed that there is no statistically significant correlation between area under CR trajectory and the position of the sample, which suggests that changes in values of considered parameter should be linked only to changes in IOP. Since both the acquisition of a B-scan as well as the measurement of IOP with air-puff tonometer occurs at the fraction of the ocular pulse period (closely corresponding to the heart rate), it is difficult to correlate the results from both instruments as in the extreme-case scenario, the OCT-evaluated IOP may be that corresponding to the peak of the ocular pulse envelope whereas that estimated with tonometry may correspond to its valley. Such difference would then amount to even several mmHg.

It is also worth noting, based on the results from section 2.3, that the statistical parameters of speckle can reflect changes in sample position, as it was observed for CR values. Area under CR trajectory was normalized by subtracting CR value from the first ROI position, so it reflects relative changes of speckle statistics and is not sensitive to sample position. The normalization of speckle parameters was applied also in other works [21,22], as it reduces the impact of changes in pixel brightness caused by external factors during imaging. In further studies on speckle statistics in OCT images, one should verify if changes in sample position are affecting values of considered parameter.

Summarizing, corneal speckle statistics in OCT images were found to be a promising tool for IOP estimation based on measurements requiring no corneal deformation. Although detailed verification on living human eyes is indispensable, it can be found as an interesting approach for the development of a new way of estimating IOP. Further, this study shows the developmental potential to yet another functionality of OCT technology.

Acknowledgments. Part of this study was presented at ARVO 2023 Meeting.

Disclosures. The authors declare no conflicts of interest.

Data availability. Data underlying the results presented in this paper are not publicly available at this time but may be obtained from the authors upon reasonable request.

References

1. R. L. Stamper, "A history of intraocular pressure and its measurement," Optom. Vis. Sci. **88**(1), E16–E28 (2011).
2. F. Silva and M. Lira, "Intraocular pressure measurement: a review," Surv. Ophthalmol. **67**(5), 1319–1331 (2022).
3. J. A. Cook, A. P. Botello, A. Elders, A. F. Ali, A. Azuara-Blanco, C. Fraser, K. McCormack, and J. M. Burr, "Systematic review of the agreement of tonometers with Goldmann applanation tonometry," Ophthalmology **119**(8), 1552–1557 (2012).
4. P. Pavlásek, J. Rybář, S. Ďuriš, B. Hučko, M. Chytil, A. Furdová, S. L. Ferková, J. Sekáč, V. Suchỳ, and P. Grosinger, "Developments and progress in non-contact eye tonometer calibration," Meas. Sci. Rev. **20**(4), 171–177 (2020).

Biomedical Optics EXPRESS

5. M.-R. Sedaghat, H. Momeni-Moghaddam, A. Yekta, A. Elsheikh, M. Khabazkhoob, R. Ambrósio Jr, N. Maddah, and Z. Danesh, "Biomechanically-corrected intraocular pressure compared to pressure measured with commonly used tonometers in normal subjects," Clin. Optom. **11**, 127–133 (2019).
6. Y. Nakao, Y. Kiuchi, and H. Okumichi, "Evaluation of biomechanically corrected intraocular pressure using Corvis ST and comparison of the Corvis ST, noncontact tonometer, and Goldmann applanation tonometer in patients with glaucoma," PLoS One **15**(9), e0238395 (2020).
7. N. G. Karyotakis, H. S. Ginis, A. I. Dastiridou, M. K. Tsilimbaris, and I. G. Pallikaris, "Manometric measurement of the outflow facility in the living human eye and its dependence on intraocular pressure," Acta Ophthalmol. **93**(5), e343–e348 (2015).
8. D. Alonso-Caneiro, K. Karnowski, B. J. Kaluzny, A. Kowalczyk, and M. Wojtkowski, "Assessment of corneal dynamics with high-speed swept source optical coherence tomography combined with an air puff system," Opt. Express **19**(15), 14188–14199 (2011).
9. A. Jiménez-Villar, E. Mączyńska, A. Cichański, M. Wojtkowski, B. J. Kałużny, and I. Grulkowski, "High-speed OCT-based ocular biometer combined with an air-puff system for determination of induced retraction-free eye dynamics," Biomed. Opt. Express **10**(7), 3663–3680 (2019).
10. E. Maczynska, K. Karnowski, K. Szulzycki, M. Malinowska, H. Dolezyczek, A. Cichanski, M. Wojtkowski, B. Kaluzny, and I. Grulkowski, "Assessment of the influence of viscoelasticity of cornea in animal ex vivo model using air-puff optical coherence tomography and corneal hysteresis," J. Biophotonics **12**(2), e201800154 (2019).
11. M. Singh, Z. Han, A. Nair, A. Schill, M. D. Twa, and K. V. Larin, "Applanation optical coherence elastography: noncontact measurement of intraocular pressure, corneal biomechanical properties, and corneal geometry with a single instrument," J. Biomed. Opt. **22**(02), 1 (2017).
12. D. A. Jesus and D. R. Iskander, "Assessment of corneal properties based on statistical modeling of OCT speckle," Biomed. Opt. Express **8**(1), 162–176 (2017).
13. D. R. Iskander, M. A. Kostyszak, D. A. Jesus, M. Majewska, M. E. Danielewska, and P. Krzyżanowska-Berkowska, "Assessing corneal speckle in optical coherence tomography: a new look at glaucomatous eyes," Optom. Vis. Sci. **97**(2), 62–67 (2020).
14. D. A. Jesus, M. Majewska, P. Krzyzanowska-Berkowska, and D. R. Iskander, "Influence of eye biometrics and corneal microstructure on noncontact tonometry," PLoS One **12**(5), e0177180 (2017).
15. M. Niemczyk, M. E. Danielewska, M. A. Kostyszak, D. Lewandowski, and D. R. Iskander, "The effect of intraocular pressure elevation and related ocular biometry changes on corneal OCT speckle distribution in porcine eyes," PLoS One **16**(3), e0249213 (2021).
16. M. Niemczyk and D. R. Iskander, "Statistical analysis of corneal OCT speckle: a non-parametric approach," Biomed. Opt. Express **12**(10), 6407–6421 (2021).
17. T. R. Hillman, S. G. Adie, V. Seemann, J. J. Armstrong, S. L. Jacques, and D. D. Sampson, "Correlation of static speckle with sample properties in optical coherence tomography," Opt. Lett. **31**(2), 190–192 (2006).
18. M. Niemczyk and D. R. Iskander, "Potential for measuring intraocular pressure using static OCT corneal images," Investigative Ophthalmology Visual Science **64**, 3365 (2023).
19. S. Bandyopadhyay, B. Ganguli, and A. Chatterjee, "A review of multivariate longitudinal data analysis," Stat. Methods Med. Res. **20**(4), 299–330 (2011).
20. M. Kohlhaas, A. G. Boehm, E. Spoerl, A. Pürsten, H. J. Grein, and L. E. Pillunat, "Effect of central corneal thickness, corneal curvature, and axial length on applanation tonometry," Arch. Ophthalmol. **124**(4), 471–476 (2006).
21. X. Y. Wang, T. Q. Zhang, A. R. Rachwani, I. Blanco-Domínguez, C. Rocha de Lossada, A. M. Adán-Civiera, and J. Peraza-Nieves, "New algorithm for corneal densitometry assessment based on anterior segment optical coherence tomography," Eye **36**(8), 1675–1680 (2022).
22. M. Vilbert, R. Bocheux, H. Lama, C. Georgeon, V. Borderie, P. Pernot, K. Irsch, and K. Plamann, "Objective assessment of corneal transparency in the clinical setting: correction of acquisition artifacts in SD-OCT images and application to normal corneas," in *European Conference on Biomedical Optics*, (Optica Publishing Group, 2021), pp. EW1C-5.
23. I. Sanchez, R. Martin, F. Ussa, and I. Fernandez-Bueno, "The parameters of the porcine eyeball," Graefe's Arch. Clin. Exp. Ophthalmol. **249**(4), 475–482 (2011).
24. B. K. Pierscionek, M. Asejczyk-Widlicka, and R. A. Schachar, "The effect of changing intraocular pressure on the corneal and scleral curvatures in the fresh porcine eye," Br. J. Ophthalmol. **91**(6), 801–803 (2007).
25. S. G. Adie, T. R. Hillman, and D. D. Sampson, "Investigation of speckle contrast ratio in optical coherence tomography," in *Complex Dynamics and Fluctuations in Biomedical Photonics III*, vol. 6085 (SPIE, 2006), pp. 29–40.
26. Z. Li, H. Li, Y. He, and C. Shoudong, "Experimental correlation of OCT speckle contrast ratio with the detectable depth and scattering coefficient of the sample," Adv. Biomed. Photonics Imaging pp. 306–308 (2008).
27. Z. Li, H. Li, Y. He, S. Cai, and S. Xie, "A model of speckle contrast in optical coherence tomography for characterizing the scattering coefficient of homogenous tissues," Phys. Med. Biol. **53**(20), 5859–5866 (2008).
28. T. M. Nguyen, J. F. Aubry, M. Fink, J. Bercoff, and M. Tanter, "*In vivo* evidence of porcine cornea anisotropy using supersonic shear wave imaging," Invest. Ophthalmol. Visual Sci. **55**(11), 7545–7552 (2014).
29. K. M. Meek and C. Knupp, "Corneal structure and transparency," Prog. Retinal Eye Res. **49**, 1–16 (2015).

Biomedical Optics EXPRESS

30. M. E. Danielewska, M. A. Kostyszak, P. Sareło, M. Gąsior-Głogowska, M. Niemczyk, P. Prządka, A. Antończyk, Z. Kiełbowicz, and D. R. Iskander, "Indirectly assessing changes in corneal properties with OCT speckle after crosslinking in porcine eyes," Exp. Eye Res. **219**, 109051 (2022).
31. A. Benoit, G. Latour, S. K. Marie-Claire, and J. M. Allain, "Simultaneous microstructural and mechanical characterization of human corneas at increasing pressure," J. Mech. Behav. Biomed. Mater. **60**, 93–105 (2016).
32. A. M. Bhorade, M. O. Gordon, B. Wilson, R. N. Weinrab, and M. A. Kass, "Variability of intraocular pressure measurements in observation participants in the ocular hypertension treatment study," Ophthalmology **116**(4), 717–724 (2009).
33. I. Goldberg and C. I. Clement, "The water drinking test," Am. J. Ophthalmol. **150**(4), 447–449 (2010).
34. S. Pourjavan, P.-Y. Boëlle, M. Detry-Morel, and P. De Potter, "Physiological diurnal variability and characteristics of the ocular pulse amplitude (OPA) with the dynamic contour tonometer (DCT-Pascal)," Int. Ophthalmol. **27**(6), 357–360 (2007).
35. C. Kaufmann, L. M. Bachmann, Y. C. Robert, and M. A. Thiel, "Ocular pulse amplitude in healthy subjects as measured by dynamic contour tonometry," Arch. Ophthalmol. **124**(8), 1104–1108 (2006).
36. S. A. Read, M. J. Collins, and D. R. Iskander, "Diurnal variation of axial length, intraocular pressure, and anterior eye biometrics," Invest. Ophthalmol. Visual Sci. **49**(7), 2911–2918 (2008).
37. D. Robert Iskander and H. T. Kasprzak, "Dynamics in longitudinal eye movements and corneal shape," Ophthalmic Physiol. Opt. **26**(6), 572–579 (2006).
38. M. A. Kowalska, H. T. Kasprzak, D. R. Iskander, M. Danielewska, and D. Mas, "Ultrasonic in vivo measurement of ocular surface expansion," IEEE Trans. Biomed. Eng. **58**(3), 674–680 (2010).
39. S. Kwok, K. Clayson, N. Hazen, X. Pan, Y. Ma, A. J. Hendershot, and J. Liu, "Heartbeat-induced corneal axial displacement and strain measured by high frequency ultrasound elastography in human volunteers," Transl. Vis. Sci. Technol. **9**(13), 33 (2020).